



The Microstructure, Surface Topography and Wear Resistance of Cold-Sprayed (Cr₃C₂-25(Ni₂₀Cr))-(Ni-graphite) Composite Coatings Modified by Diode Laser Treatment

Anna Trelka-Druzic¹ · Wojciech Żórawski² · Lidia Lityńska-Dobrzyńska¹ · Łukasz Maj¹ · Marcin Kot³ · Grzegorz Wiązania³ · Anna Góral¹

Submitted: 11 January 2024 / in revised form: 30 April 2024 / Accepted: 12 May 2024
© The Author(s) 2024

Abstract Cold-sprayed composite coatings have several advantages; however, some properties, such as hardness and abrasion resistance, are lower than those in plasma- or HVOF-sprayed deposits. This work showed that the use of surface diode laser processing allowed the development of (Cr₃C₂-25(Ni₂₀Cr))-(Ni-graphite) cermet coatings with good adhesion to the steel substrate, and increased properties in the near-surface zone, below which the properties of cold-sprayed coatings were retained. Studies of the microstructure in the micro/nanoscale of the laser-treated coatings showed strong grain refinement after surface treatment. Cr₇C₃ carbide of various shapes and sizes was formed in the structure; while, a several hundred nanometre layer of Cr₂O₃ oxide appeared on the coating surface. The changes occurring in the microstructure have resulted in increased mechanical and tribological properties of the laser-treated zone of deposits.

Keywords cermet coating · cold spraying · microstructure · surface laser treatment · tribological properties

Introduction

Composite coatings have recently become popular in the automotive, aviation and printing industries. Most often, such coatings are produced using thermal spraying methods: plasma spray, HVOF and cold spray. The latter are characterised by numerous advantages compared to coatings sprayed using the plasma (PS) and high velocity oxy fuel (HVOF) methods, primarily the lack of change in the phase composition (Ref 1-3).

Plasma-sprayed and HVOF Cr₃C₂-(Ni-Cr) coatings are characterised by partially dissolved carbides and a chromium enriched Ni-Cr matrix. Additionally, dissolved carbide can be lost as carbon monoxide or carbon dioxide, increasing the formation of Cr₇C₃ and Cr₂₃C₆ carbides. These processes result in deposit formation with higher porosity and lower adhesion compared to that of cold-sprayed ones (Ref 4-6). To improve the properties of plasma- and HVOF-sprayed coatings, surface laser treatment is performed. This modification leads to grain refinement in the structure, reduces roughness and improves the mechanical and tribological properties of the coatings. However, this treatment causes significant changes in the phase composition.

Cold-sprayed (Cr₃C₂-25(Ni₂₀Cr))-5(Ni₂₅C) cermet deposits, through the use of hard Cr₃C₂ ceramic particles and a plastic Ni₂₀Cr matrix, ensure high hardness and a compact structure. The coatings are characterised by negligible porosity, a homogeneous structure and low residual stresses. They are formed by mechanical interlocking and

✉ Anna Trelka-Druzic
a.trelka@imim.pl

✉ Anna Góral
a.goral@imim.pl

¹ Institute of Metallurgy and Materials Science, Polish Academy of Sciences, 25 Reymonta St., 30-059 Krakow, Poland

² Faculty of Mechatronics and Mechanical Engineering, Kielce University of Technology, Tysiąclecia Państwa Polskiego 7, 25-314 Kielce, Poland

³ Laboratory of Surface Engineering and Tribology, Faculty of Mechanical Engineering and Robotics, AGH University of Science and Technology, Mickiewicza 30 Ave. (B2), 30-059 Krakow, Poland

adiabatic shear instability, which provide high adhesion to the substrates. The addition of a solid lubricant in the form of graphite improves the tribological properties of coatings (Ref 7). The laser treatment of cold-sprayed coatings increases the mechanical and tribological properties of the surface layer, allowing deposits without porosity and with strong coating–substrate bonding, in contrast to plasma- or HVOF-sprayed coatings, where there is a thermo-mechanical connection. It is also worth mentioning the negative aspects of the laser melting process, which is the cracking of the material. The appearance of cracks in laser-melted material is related to the melting and rapid crystallisation of the surface layer. We can distinguish two types of cracking: hot and cold. Hot cracks occur when there are low-melting elements in the structure of the remelted material when there is a non-uniform distribution of brittle phases and impurities, and during disordered grain growth. Tensile stresses occur in the structure, which is the result of rapid subcooling of the liquid metal in a very high-temperature pool. The resulting tensile stresses mean that the liquid phase is unable to fill the emerging gaps, which causes further cracking of the material (Ref 8, 9). Cold cracks are a more common phenomenon and are related to improper selection of melting process parameters and excessive temperature gradient in the melt pool. Differences in the thermophysical parameters of the coating material and the substrate, combined with the cooling and solidification process, result in large residual thermal stresses. When these stresses exceed the tensile strength limit of the material, cold cracks appear (Ref 10, 11).

The literature reports indicate that cold-sprayed $\text{Cr}_3\text{C}_2\text{-}25(\text{Ni}20\text{Cr})$ coatings have been treated with CO_2 and Nd:YAG lasers so far (Ref 12, 13). In this work, the processing was performed using a diode laser. Compared to other lasers used for laser hardening (CO_2 and Nd:YAG), diode lasers have the advantage of emitting a shorter wavelength (808 nm and/or 940 nm) that is better absorbed by metals and excellent process stability. Additionally, diode lasers do not require special absorption layers, which may prevent temperature control by a pyrometer and may also cause surface contamination. Due to the high efficiency of diode lasers, as well as the beam profile, lower investment and operating costs compared to the Nd:YAG laser, they are preferred for the surface treatment of materials (Ref 14). There are several papers describing the use of diode lasers to remelt the surface layer of coatings produced by thermal spraying (Ref 15–17). Grimm et al. (Ref 15) investigated three-component plasma-sprayed oxide coatings subjected to surface modification using a diode laser. The tests showed a change in the phase composition of the coatings and an increase in hardness after laser treatment. Morimoto et al. (Ref 16) examined coatings sprayed supersonically and then subjected to laser

surface treatment using a diode laser. Microhardness and wear resistance tests confirmed that the modified coatings revealed better mechanical and tribological properties. WC-12Co coatings sprayed supersonically and then subjected to laser surface modification using a diode laser showed up to 50% higher hardness and Young's modulus in the modified zone, and higher scratch resistance (Ref 17). As shown in the literature (Ref 12, 13, 15, 16), laser modification is mainly aimed at improvement by eliminating the porosity of the coatings, and changing the phase composition, whilst in cold-sprayed ones, apart from modifying the phase composition of this zone, a fine-grained structure can be obtained. From the application perspective, it is important that coatings can be characterised by high hardness, wear resistance, low friction coefficient and a compact structure in the usable zone, while maintaining high adhesion. These expectations can be met by cold-sprayed cermet coatings and subjected to laser surface treatment because, in the modified zone, they have good mechanical and tribological properties, whereas below they are characterised by a compact structure without pores and good adhesion with the substrate, which results from the metallurgical bond that is formed by adiabatic shear instability and mechanical interlocking mechanisms (Ref 7, 18).

Cold-sprayed ($\text{Cr}_3\text{C}_2\text{-}25(\text{Ni}20\text{Cr})\text{-}5(\text{Ni}25\text{C})$) coatings later modified using a diode laser have not been tested so far, which constitutes a knowledge gap. The work presents novelty aspects: (1) creating and characterisation of the cermet coatings, which are characterised by good mechanical and tribological properties in the laser remelted surface layer below which they possess a compact composite structure obtained using cold-spraying technique, (2) analysis of mechanical and tribological properties taking into account changes occurring in the deposit microstructure in the micro- and nano-scale, especially in the modified surface.

Materials and Manufacturing

The composite coatings were produced using commercially available powders: $\text{Cr}_3\text{C}_2\text{-}25(\text{Ni}20\text{Cr})$ Diamalloy 3004 and Ni25C Durabrade 2221, manufactured by Oerlikon-Metco GmbH, Immelborn, Germany (in the ratio 95 wt.%–5 wt.%) on a 1H18N9T steel substrate (flat bar with dimensions of 400 mm x 30 mm x 5 mm). The cold spray process was carried out with an Impact Innovations 5/8 Cold Spray System, mounted on a Fanuc M-20iA robot arm (Impact Innovations GmbH, Rattenkirchen, Germany). Table 1 shows the parameters of the cold spray process.

The cold-sprayed coatings were treated using a Laserline diode laser (Laserline GmbH, Mülheim-Kärlich,

Table 1 Parameters of the cold spray process

Parameter	Value
Working gas	45% N ₂ + 55% He
Gas pressure, MPa	4
Temperature, °C	800
Powder feeder rate, g/mm	95 ± 3
Standoff distance, mm	23
Step size, mm	2
Number passes	15
Number of layers	3

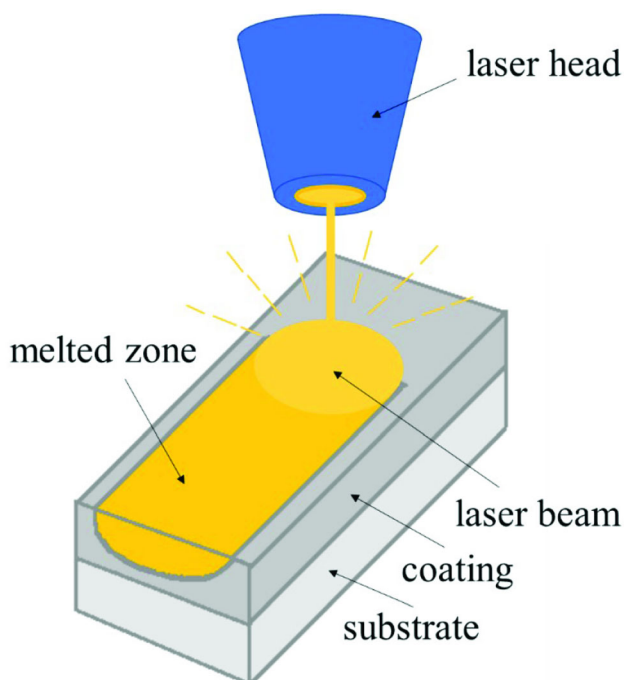
Table 2 Parameters of diode laser treatment

Parameter	Value
Size of laser beam, mm x mm	10 x 1
Laser power, kW	4
Velocity of laser beam, mm/s	33
Power density of laser beam, (J/mm ³) 10 ⁴	121

Experimental Methods

In this work, several tests were performed to determine how laser processing affects the microstructure, mechanical and tribological properties of cold-sprayed (Cr₃C₂)-25(Ni20Cr)-5(Ni25C) cermet coatings. Figure 2 shows the plan of the analysed aspects of the work and the experimental methods used.

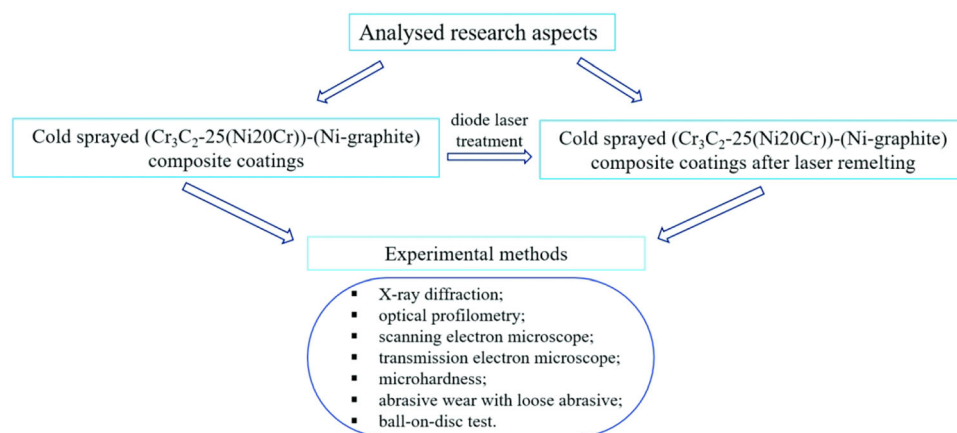
The phase composition of the as-sprayed and laser-treated coatings was investigated using a Bruker D8 Discover diffractometer (Bruker AXS GmbH, Karlsruhe, Germany) with CoK α radiation and Diffrac.EVA software with the ICDD PDF-4 + crystallographic database. The microstructure and chemical composition were studied using a scanning electron microscope (FEI /Philips XL30, FEI Company, Oregon, United States) and an FEI TECNAI G2 TEM transmission electron microscope (FEI Company, Hillsboro, Oregon, USA), equipped with an SIS MegaView III CCD camera for the acquisition of the microstructure images in bright-field mode and the recording of selected-area electron diffraction patterns (SAED). The chemical composition was analysed with an energy-dispersive EDAX X-ray spectrometer. Phase analysis based on electron diffraction patterns in TEM was investigated using Carine V3 computer software. The thin foils for transmission electron microscopy studies were cut with the FIB technique using an FEI QUANTA 3D Dual Beam (FEI Company, Hillsboro, Oregon, USA). The surface topography of the as-sprayed and laser-treated coatings was tested with a profilometer (Filmetrics Profilom 3D, KLA Corporation, Milpitas, California, USA). The device uses White Light Interferometry technique for capturing surface geometry. Geometry was measured with x40 magnification with spatial sampling 0.88 μ m and height measure accuracy 0.06 μ m. The geometrical parameters of the coatings were measured according to the ISO 25178 standard (Ref 19). An Innovatest low-load Vickers hardness tester (HV0.3) was used to determine the coating hardness on the cross section (Innovatest Europe BV, Maastricht, The Netherlands). In each case, the hardness result was an average of 15 measurements taken at different points. The coating hardness was measured in accordance with the ISO

**Fig. 1** Diagram of the coating remelting process

Germany). The laser treatment parameters were selected to allow for remelting the coatings in the surface layer without affecting the coating–substrate interface. The laser-processed area in the coating is shown in Figure 1.

The parameters, such as laser type, laser power, velocity of laser beam, and shape and size of the laser beam, significantly influenced the depth of treatment and the quality of the remelted zone. Argon was used as a shielding gas. The key task was to eliminate round pores in the structure created by gas bubbles formed during remelting, which didn't manage to reach the surface and cracking appearing during process. The optimal parameters of laser treatment were chosen based on the tests carried out for various process conditions and structure analysis of the treated coatings. They are presented in Table 2.

Fig. 2 Plan of the experiments performed



6507- 1:2018(en) standard (Ref 20). Hardness was measured according to the diagonal of the imprint. The abrasive wear tests were performed using an ITEE T-07 tester (The Institute for Sustainable Technologies, Radom, Poland) (dry sand-rubber wheel) and loose abrasive Al_2O_3 particles 250 μm to 300 μm in size, at a flow rate of 250 g/min, a wheel ($\text{Ø}50 \times 20$) rotation speed of 200 rpm, and a load of 90 N. The microstructure after the abrasive wear tests were visualised using a Leica optical microscope. Tests of the wear index and the friction coefficient of coatings were carried out with the use of a ball-on-disc T-21 tribotester (The Institute for Sustainable Technologies, Radom, Poland). The ball was a 6 mm-diameter sintered Si_3N_4 sphere, its linear sliding speed was 0.1 m/s, the radii were 5, 7, and 8.5 mm, and the number of cycles was 20000. The investigations were performed under two loads of 10 N and 15 N and at three temperatures of 25 °C, 250 °C and 500 °C in heated ambient air and at atmospheric pressure for as-sprayed and laser-treated deposits. The chamber was heated with the samples and the temperature was maintained for one hour using a thermocouple. The friction and wear characteristics were tested in accordance with the ISO 20808:2016(E) standard (21). The coating surface was ground and polished on diamond polishing suspensions with a finishing gradation of 1 μm .

Phase Composition of Coatings

The phase composition of the $(\text{Cr}_3\text{C}_2\text{-}25(\text{Ni}20\text{Cr}))\text{-}5(\text{Ni}25\text{C})$ coatings revealed the presence of the $\text{Cr}_{0.25}\text{Ni}_{0.75}$ matrix, Cr_3C_2 carbide, Ni and C (graphite) (Fig. 3). The coatings showed no changes in phase composition compared to the feedstock powders, as tested in previous studies (Ref 7, 12). The laser-treated deposits showed new phases, such as Cr_7C_3 and Cr_2O_3 . The existence of the above-mentioned phases indicates that the coating treatment caused a partial dissolution of the Cr_3C_2 carbide in

the $\text{Cr}_{0.25}\text{Ni}_{0.75}$ matrix and, as a result, the formation of Cr_7C_3 carbide. The appearance of the oxide phases indicates the oxidation of the coating during the laser treatment.

Surface Topography of Coatings

Coating surface topography measured using an optical profilometer in accordance with ISO 25178 showed higher roughness parameter for laser-treated coatings (Table 3). In the laser-melted deposits single pores of up to several dozen micrometres were visible on the surface, as shown by the surface contour map and the 3D isometric image (Fig. 4). This resulted in an increase in the value of the S_a parameter of the laser-melted coating by approximately 30% compared to the sprayed coating. The appearance of holes on the surface is the result of the release of CO_2 gas resulting from the oxidation of graphite in the coating (Ref 12). The roughness parameters of the laser-melted coating were also tested in the zone where there were no holes on the surface (a rectangular area indicated by the arrow in Fig 4c). In this case, they were characterised by 30% lower surface roughness (S_a) compared to the sprayed coatings. This confirms that the laser melting process generally smooths the coating surface when skipping the holes.

Microstructures of $(\text{Cr}_3\text{C}_2\text{-}25(\text{Ni}20\text{Cr}))\text{-}(\text{Ni-Graphite})$ Coatings

SEM Microstructures of Deposits

The morphology of the cold-sprayed coatings examined using scanning electron microscopy showed a highly deformed Ni-Cr metallic phase and embedded ceramic particles (Fig. 5a). A higher roughness surface was observed compared to the laser-melted coating, which was

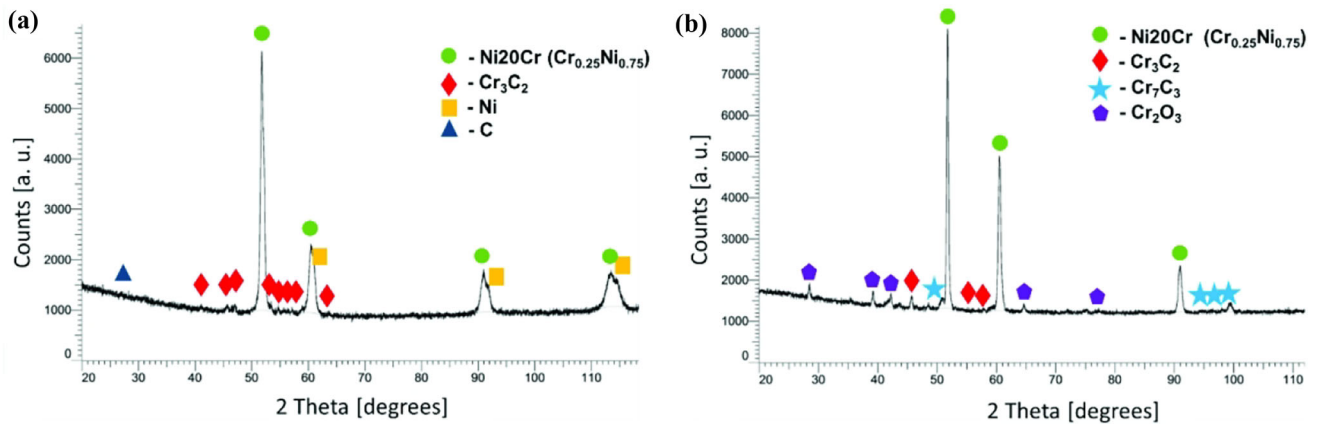


Fig. 3 Phase composition of the cold-sprayed (Cr₃C₂-25(Ni20Cr))-5(Ni25C) (a) and laser-treated (b) deposits

Table 3 Coating surface topography parameters according to ISO 25178 (19)

Coatings	Surface roughness parameters	Sa (Arithmetic mean height), μm	Sp (Maximum peak height), μm	Sv (Maximum pit height), μm	Sz (Maximum height), μm	Sq (Root mean square height), μm	Ss, Skewness	Sk, Kurtosis
As-sprayed		9.35	39.83	53.71	93.53	11.66	- 0.15	2.94
Laser-treated	Entire area	12.96	68.71	97.41	166.10	18.68	- 0.95	7.75
	Area indicated by arrow	7.55	33.91	47.68	81.59	9.91	- 0.29	4.46

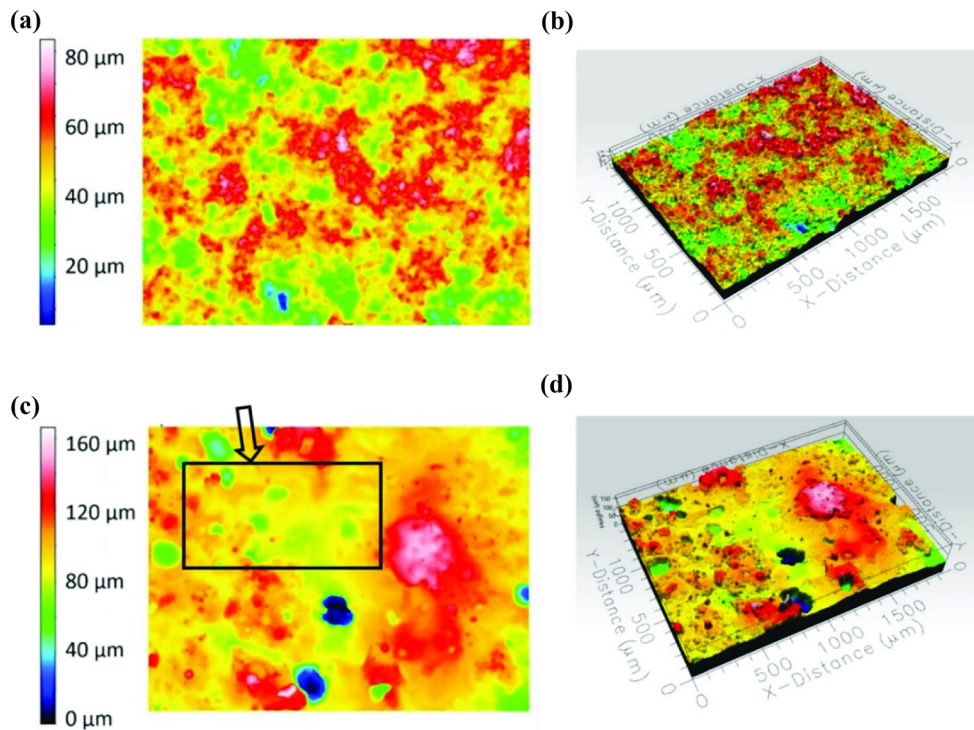


Fig. 4 Surface contour maps (a, c) and 3D isometric images (b, d) of the as-sprayed (a, b) and laser-treated coatings (c, d)

characterised by lower roughness. The SEM morphology of the laser-treated coating surface is shown in Figure 5d and 6. On the coating surface after laser melting, a thin,

uneven oxide layer was formed, which inhibited further interaction of oxygen with the coating. Its occurrence may suggest that it was formed in Cr-rich areas resulting from

Fig 5 SEM-BSE surface morphologies and cross sections of the as-sprayed (a,b,c) and laser-treated (d, e, f) deposits

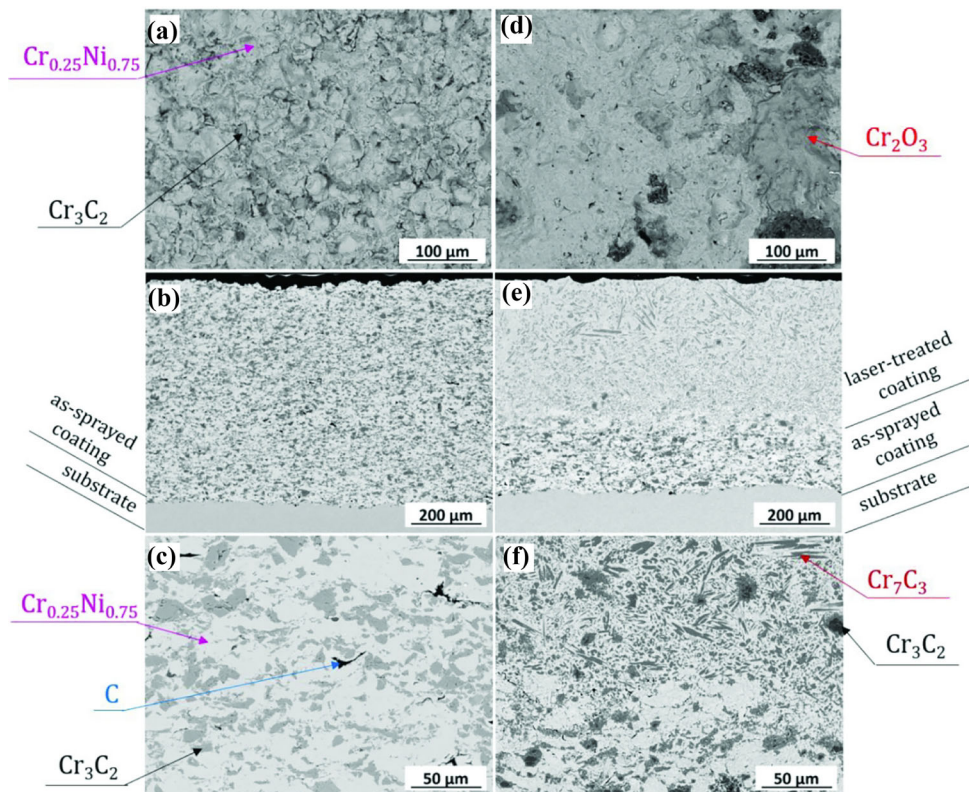
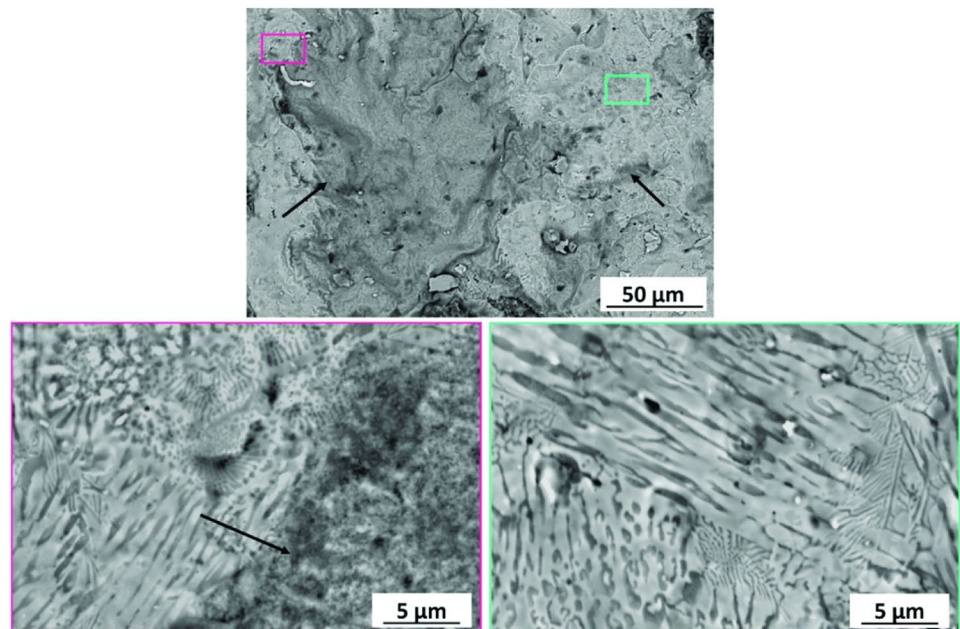


Fig. 6 High magnification SEM-BSE surface morphologies of laser-treated coatings (arrow indicates Cr_2O_3)



the dissolution of Cr_3C_2 in the matrix. Cr_2O_3 oxide (dark grey areas) was formed on the coating surface by oxidation of Cr due to the direct contact of air with the sample surface. Unlike the sprayed coatings, no embedded Cr_3C_2 ceramic particles and no deformed particles were observed in the modified zone. The light phase visible on the surface

appeared homogeneous, but a microstructure at higher magnification showed the presence of areas composed of alternating dark and light phases.

In the cross section of the sprayed coating, an evenly distributed ceramic phase and graphite in the metal matrix are observed. The coatings are characterised by negligible

porosity, and there are no visible discontinuities in the zone near the substrate (Fig. 5b). Microstructure of the cross section of the Cr_3C_2 -25(Ni20Cr)-5(Ni25C) coating after laser modification indicated that the coating was melted to a thickness of approximately 60% (Fig. 5e). In the boundary zone of the coating between the remelted and unmodified part (Fig. 5f), Cr_3C_2 carbides were visible, which were partially remelted while retaining the Cr_3C_2 carbide core. The small carbides were completely melted. The microstructure created as a result of complete melting of the original structure consisted of newly-formed Cr_7C_3 carbides and the $\text{Cr}_{0.25}\text{Ni}_{0.75}$ phase. During surface modification, there was a complete or partial (with the preservation of the core) transformation of Cr_3C_2 carbide into Cr_7C_3 carbide. A supersaturation phenomenon occurred, which resulted in the subsequent formation of new Cr_7C_3 carbides during rapid crystallisation, which may indicate that it was a more energetically favourable process under these conditions than the formation of equilibrium Cr_3C_2 .

The cross section microstructure observation of the laser-treated coating performed at higher magnifications (Fig. 7) showed that it was composed of nickel–chromium phase and Cr_7C_3 carbides. Cr_7C_3 carbide existed in various forms, i.e. large elongated lamellas, several micrometre precipitates and thin lamellas with a nanometric structure. The structure of the coating consisted of larger Cr_7C_3 particles, between which alternating nanometric light ($\text{Cr}_{0.25}\text{Ni}_{0.75}$) and dark (Cr_7C_3) lamellas were arranged. In the case of large ceramic particles, a Cr_3C_2 carbide core can be observed (Fig. 7).

Both on the cross section and the surface, no cracks or discontinuities resulting from melting and crystallisation of

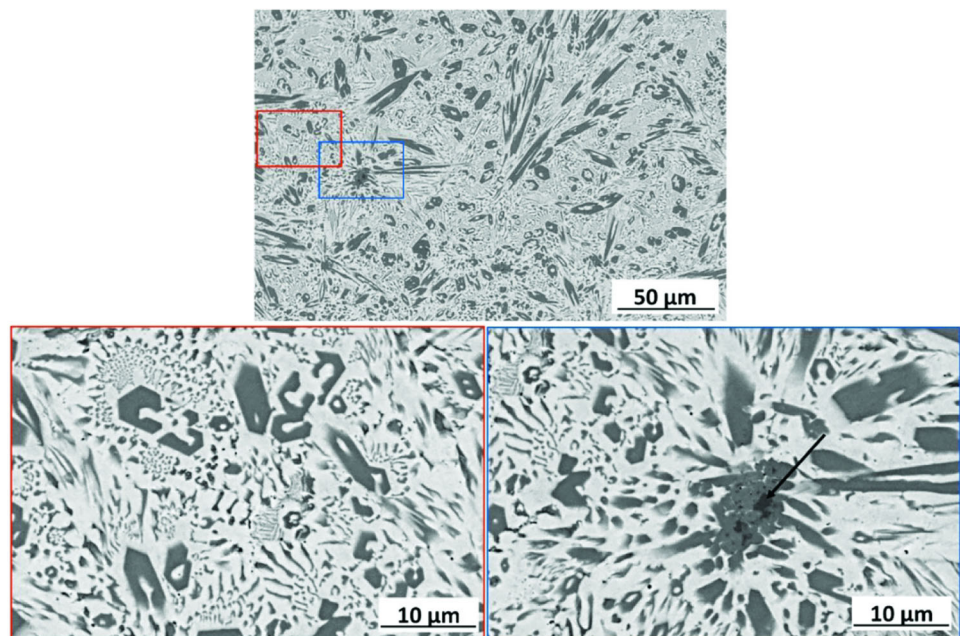
the material subjected to laser surface treatment were observed in the microstructure of the coatings (Fig. 5, 6 and 7).

TEM Microstructures and Chemical Composition of Deposits

The microstructure of laser-modified coatings observed in the micro/nano-scale using TEM is presented in Figure 8 and 9. Coatings were analysed both in the central part of the modified area (Fig. 8) and near the surface zone (Fig. 9). In the central part, the coating was composed mainly of newly-formed Cr_7C_3 carbide of various shapes and sizes, between which there was a $\text{Cr}_{0.25}\text{Ni}_{0.75}$ phase. Figure 8a indicates the presence of elongated grains of Cr_7C_3 carbide with a length of several micrometres and a width of about a micrometre; while, Figure 8b indicates the presence of this type of carbide in the form of finer grains of irregular shape. The phase composition of the coating examined using electron diffraction corresponded to the phase composition examined using X-ray diffraction (Fig. 3). In order to determine the chemical composition in the micro-areas of coatings subjected to laser surface modification, maps of the distribution of chemical elements were made (Fig. 8(b) and (d)). Chromium, nickel and carbon are located in the structure. The presence of chromium and carbon in the same areas confirmed the presence of chromium carbides of various shapes and sizes in the structure.

The presence of chromium oxides in the structure of the coatings was confirmed using X-ray diffraction. To identify their presence on the surface of the modified area, analysis of the phase composition was performed based on SAED diffraction images and the chemical composition of the area

Fig. 7 High magnification SEM-BSE cross section of laser-treated coatings (arrow indicated Cr_3C_2)



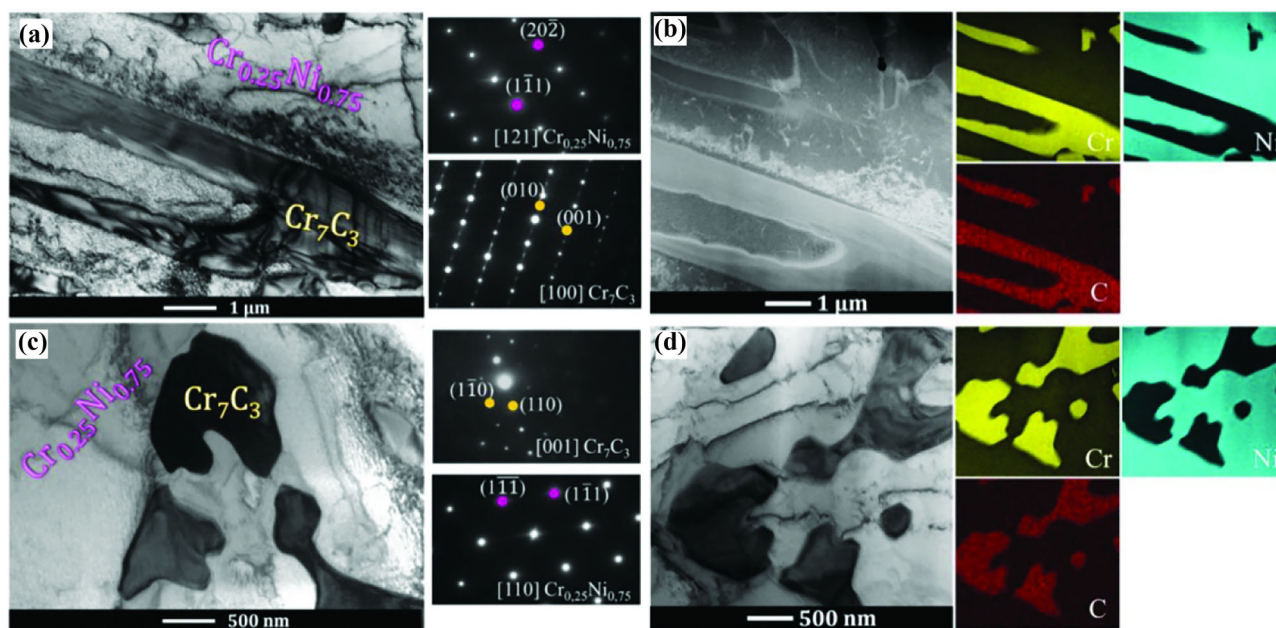


Fig. 8 TEM-BF images of the laser-treated coating (a, c) and STEM-HAADF images and chemical composition maps in the central part of the coating after laser surface treatment (b, d)

near the surface (Fig. 9). The tests performed showed the presence of a thin layer of chromium oxide Cr_2O_3 , approximately 200 nm, which was formed on the coating surface.

Mechanical Properties of Coatings

The HV0.3 microhardness measured on the cross section of the modified coating was 740 ± 29 HV, while that of the cold-sprayed coating was 607 ± 48 HV, which indicates a 20% increase in this value caused by laser treatment. The higher microhardness of the coating results from the refinement of its structure and the presence of a larger number of grain boundaries. Although Cr_7C_3 carbide has a lower microhardness compared to Cr_3C_2 carbide, the large variety of its forms and sizes (from several nanometres to several micrometres) and even distribution in the coating had a positive impact on the increase in hardness. The increase in microhardness may also be related to the structure formation process after laser treatment significantly different from that of cold-sprayed one.

Wear Resistance and Tribological Properties of Coatings

Abrasive Wear with Loose Abrasive

The abrasive wear test with loose abrasive showed approximately 30% lower mass loss of (Cr_3C_2 -25-

(Ni20Cr)-(Ni-graphite) coatings after laser surface modification in comparison with the non-treated one. Regardless of the test duration, the remelted coating was characterised by lower weight loss compared to the as-sprayed coating. After 10 minutes of the test, the mass loss of the coating was 24 mg, with a gradual increase of about 20 mg with each measured test, resulting in about 110 mg of coating mass loss after 50 minutes (Fig. 10).

Ball-on-Disc Test-Wear Index

The ball-on-disc tests were performed at temperatures of 25 °C, 250 °C and 500 °C under loads of 10 N and 15 N. Figure 11 shows the determined values of the wear index W_v for as-sprayed and laser-modified coatings.

The tests performed showed that the lowest wear index was observed for cold-sprayed coatings, tested at a temperature of 500 °C under a load of 10 N. Then, the lowest wear index was observed for laser-treated coatings, tested at a temperature of 25 °C. As the test temperature increased, an increase in the wear index of coatings after laser modification was observed. These values were comparable, regardless of the temperature used (250 °C or 500 °C) and ranged from $40.7 \cdot 10^{-6} \text{ m}^3/\text{Nm}$ to $42.3 \cdot 10^{-6} \text{ m}^3/\text{Nm}$. The highest wear index was observed for the as-sprayed deposit at 250 °C, regardless of the load used.

To illustrate the wear paths of the coatings and their profiles, selected samples were tested after ball-on-disc tests using an optical profilometer. Figure 12 shows wear path profiles of coatings after laser melting obtained for a

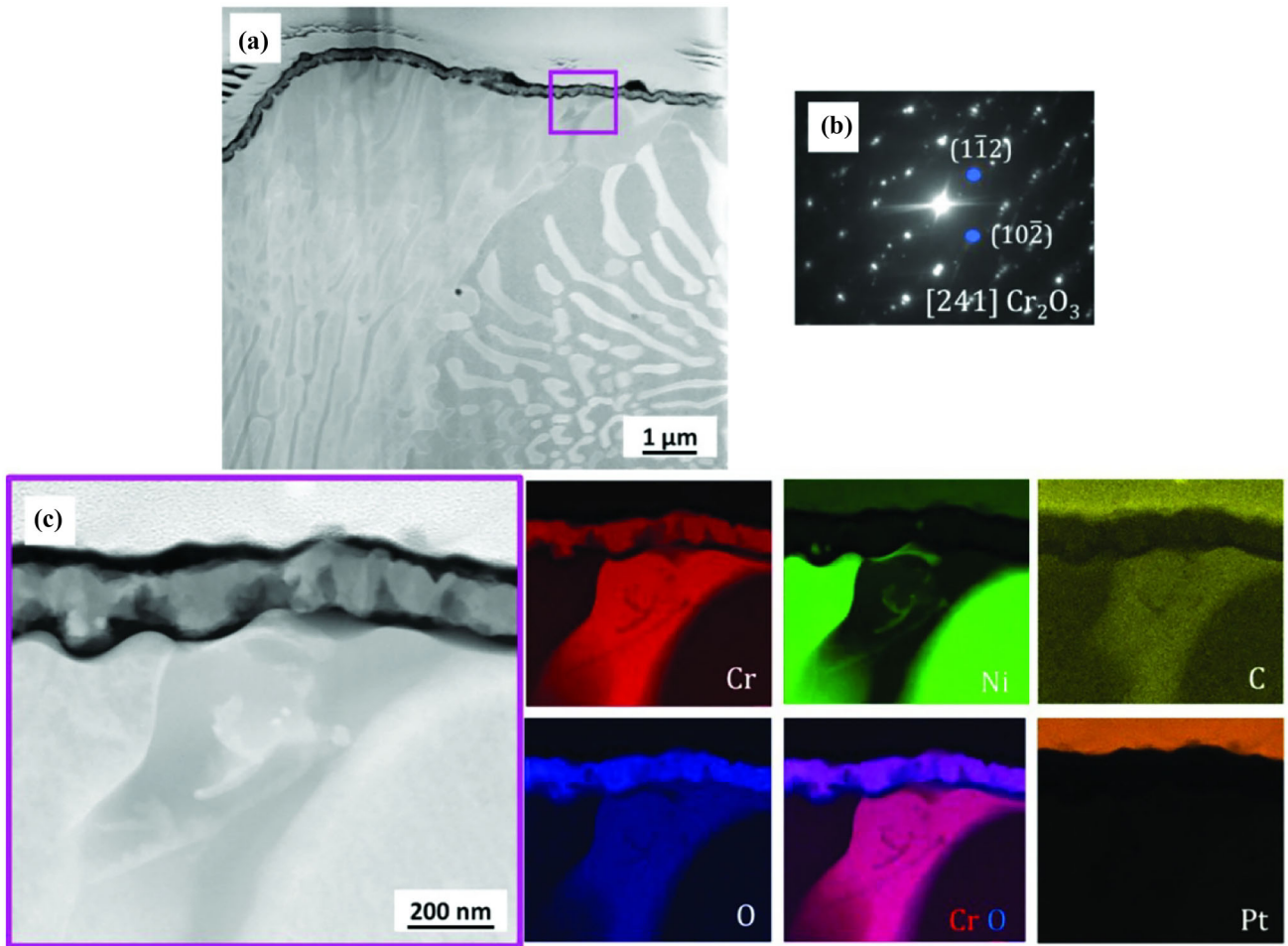


Fig. 9 STEM-HAADF images of the laser-treated coating in the near-surface region (a), electron diffraction of Cr_2O_3 oxide (b), and chemical composition maps (c)

Fig. 10 Weight loss versus time measured for the $(\text{Cr}_3\text{C}_2-25(\text{Ni}20\text{Cr}))-5(\text{Ni}25\text{C})$ coating before and after laser treatment

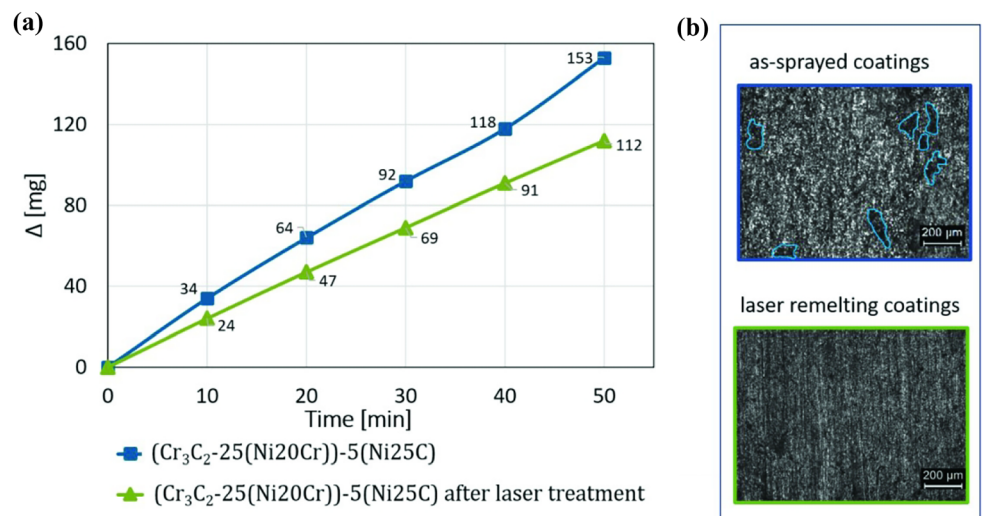
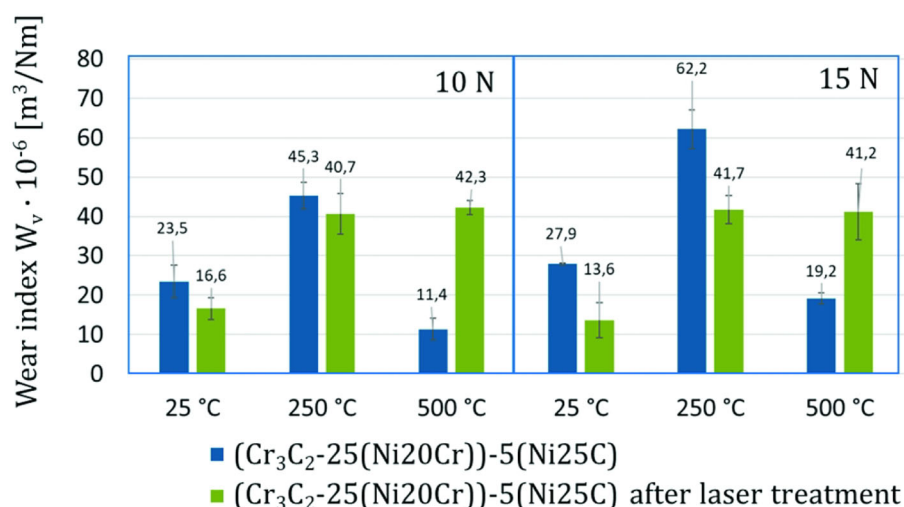


Fig. 11 Wear index of the $(\text{Cr}_3\text{C}_2\text{-}25(\text{Ni}20\text{Cr}))\text{-}5(\text{Ni}25\text{C})$ coatings before and after laser remelting, determined under various conditions



15 N load, compared with the profiles of unmodified coatings.

The presented wear paths and the profiles made on their basis reflect the coating wear index presented in Fig. 11. The coating with the lowest wear index had the narrowest and shallowest profile shape. In turn, the deepest wear profile was identified in the as-sprayed coating, tested at a temperature of 250 °C.

Ball-on-Disc Tests-Friction Coefficient

The results of the friction coefficient testing of coatings before and after laser modification at various temperatures and load variants are presented in Figure 13.

The ball-on-disc tests showed higher friction coefficients for the coatings tested at 25 °C compared to the coatings tested at elevated temperatures of 250 °C and 500 °C. During tests using a load of 10 N, a slightly higher friction coefficient was observed for laser-melted coatings tested at 25 °C and 500 °C. The opposite effect was demonstrated by coatings tested under a load of 15 N. The lowest friction coefficients were observed in coatings tested at a temperature of 500 °C and under a load of 10 N.

In order to show the characteristics of changes occurring during friction coefficient tests, Figure 14 shows the curves recorded during these measurements using a 10 N load. The highest value of the friction coefficient maintained during the tests was for the coating subjected to laser surface modification at a temperature of 25 °C. The shape of the curve is uniform throughout the entire measurement cycle. At the same measurement temperature, the friction coefficient for the as-sprayed coating showed a slightly lower value. Characteristic changes (jumps) on the curve were observed at approximately 7000 cycles and 16000 cycles. In the case of coatings tested at 500 °C, the friction coefficient curves also correspond to the values shown in

Figure 13 and confirm their lowest value. In the initial stages of testing (up to 4000 cycles), an increase in the friction coefficient value up to 0.5 was observed. This is related to the lapping effect of the sample and counter-sample occurring during the stabilisation of the system. Then it decreased and remained at the level of approximately 0.38 for the laser-melted coating and 0.36 for the unmodified one.

Discussion

Laser treatment was aimed at modifying composite coatings $(\text{Cr}_3\text{C}_2\text{-}25(\text{Ni}20\text{Cr}))\text{-}5(\text{Ni}25\text{C})$ in such a way as to improve their mechanical and tribological properties in the near-surface layer, while maintaining the structure and properties of cold-sprayed coatings near the coating–substrate interface. Surface treatment of cermet coatings based on a NiCr metal matrix Cr_3C_2 ceramic phase was performed using a diode laser, which is the most frequently recommended device for the surface hardening of materials (Ref 14). The coating was melted in the surface zone of the sprayed layer, without disturbing the connection between the coating and the substrate. Figure 15 shows the coating after laser modification. Evenly distributed oxide phases and few pores are visible on the surface. The melted zone is characterised by a highly grain refined microstructure. Below the laser-treated zone, an area of the as-sprayed coating deposited on the substrate is presented.

Phase analysis of $(\text{Cr}_3\text{C}_2\text{-}25(\text{Ni}20\text{Cr}))\text{-}5(\text{Ni}25\text{C})$ coatings subjected to laser surface treatment showed the presence of two new phases in the structure: Cr_7C_3 carbide and Cr_2O_3 oxide (Fig. 3). Changes in phase composition were reflected in the surface morphology and cross sections of the coatings (Fig. 5, 6 and 7). The Cr_2O_3 oxide was observed on their surface, which was created by combining

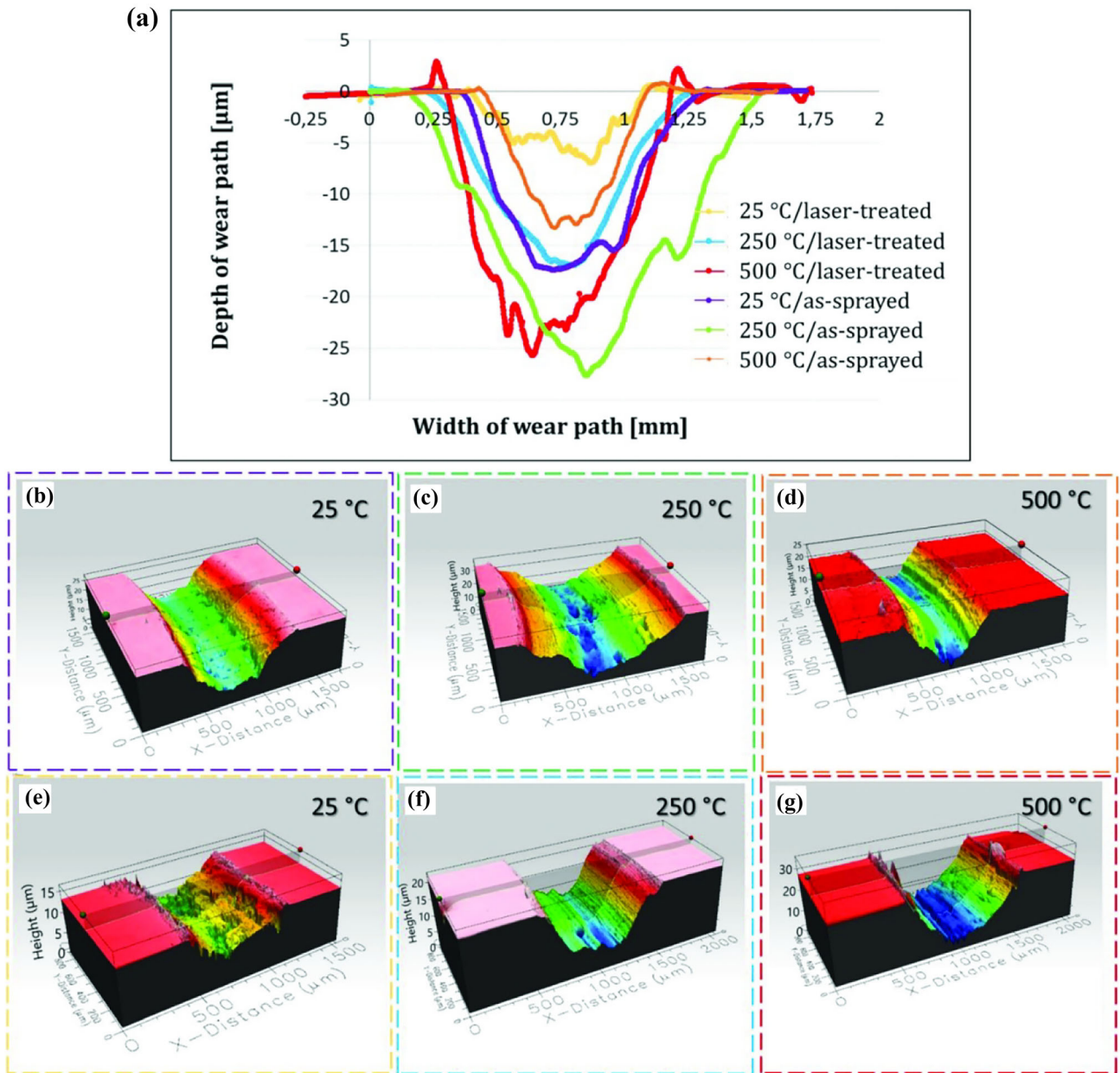


Fig. 12 Surface topography of wear paths of the $(Cr_3C_2-25(Ni20Cr))-(Ni25C)$ coatings tested under a 15 N load; depth vs. width of the deposit wear paths (a), as-sprayed coating at 25 °C (b), 250 °C (c), 500 °C (d), and laser-treated coating at 25 °C, 250 °C (f), 500 °C (g)

chromium with oxygen from the air. The thickness of this layer ranged from 20 nm - lighter areas of the surface to 200 nm - darker areas (Fig. 5 and 6). The oxide was identified only on the deposit surface, which may suggest that inhibited the interaction of oxygen with coating layers. The thickness of the oxide layer was different, which may suggest that its thicker layer was formed in Cr-rich areas, formed by dissolving Cr_3C_2 carbides in the $Cr_{0,25}Ni_{0,75}$ matrix (Ref 22, 23). Cr_2O_3 is a thermodynamically stable phase up to 1000 °C under atmospheric conditions. This phase was often formed in thermally sprayed Cr_3C_2-

NiCr coatings in the form of small oxides distributed in the structure of the coatings (Ref 22), but its presence in the structure of the coatings had an adverse effect on their mechanical and chemical properties (Ref 13).

The roughness of the $(Cr_3C_2-25(Ni20Cr))-5(Ni25C)$ coatings after laser remelting was approximately 30% higher compared to the coatings before treatment, which was caused by the presence of holes on their surface, resulting from the release of gases during the melting of the coating (Table 3 and Fig. 4). The roughness of the laser-modified coating was also measured in the zone that did not

Fig. 13 Friction coefficient of the $(Cr_3C_2-25(Ni20Cr))-(Ni25C)$ coatings before and after laser remelting, determined under various conditions

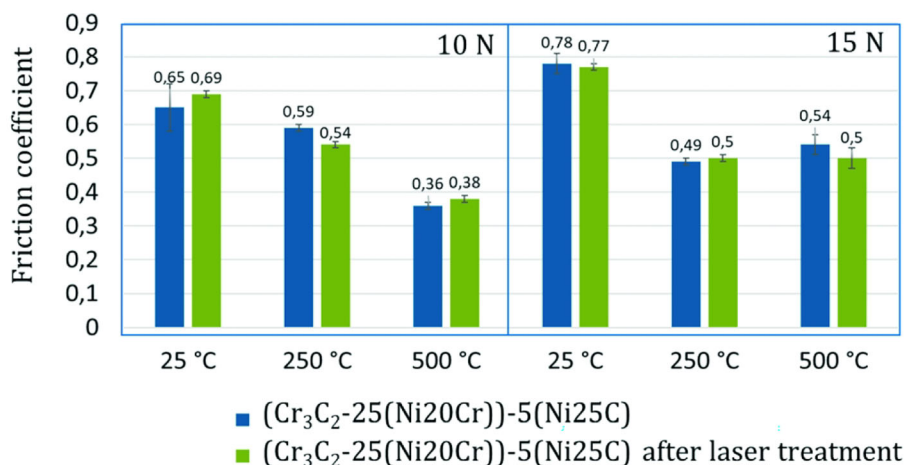


Fig. 14 Course of the coating friction coefficient curves of the $(Cr_3C_2-25(Ni20Cr))-(Ni25C)$ coatings before and after laser remelting, measured under a 10 N load and at various temperatures

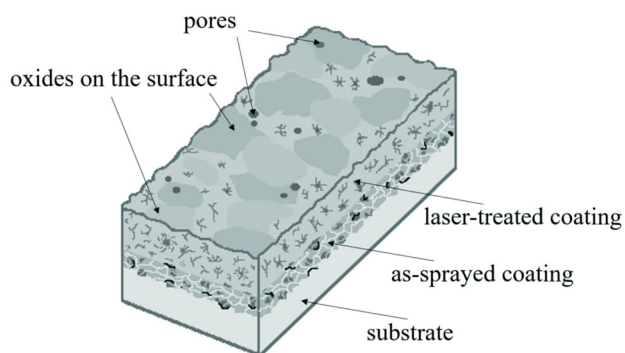
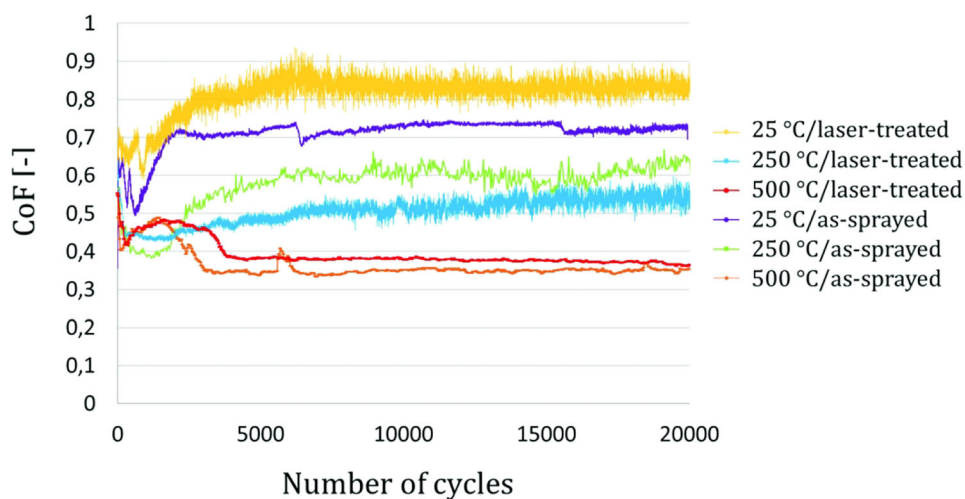


Fig. 15 $(Cr_3C_2-25(Ni20Cr))-(Ni-graphite)$ laser-treated coating

include any locally formed holes. In this area, the roughness parameters of the coatings were approximately 30% lower compared to the coatings before modification. Apart from a few holes on the coating surface, no defects in the form of cracks were observed resulting from inappropriate selection of process parameters and excessive temperature gradient in the pool. During laser remelting, small Cr_3C_2

carbides were completely dissolved in the nickel–chromium phase, leading to its supersaturation with chromium, as indicated by approximately 25% higher content of this element in these areas measured using SEM-EDS. Similarly to this work, supersaturation of the matrix leading to the precipitation of new phases was observed in materials produced by thermal spraying processes (Ref 24, 25). SEM-BSE observations of the coating surfaces at higher magnifications allowed dark and light phases to be distinguished, suggesting the presence of carbide and nickel–chromium phases. These phases were arranged alternately or appeared in an irregular form (Fig. 6). In the cross sections of the coatings, the carbide phase was characterised by various shapes and sizes. The size of the carbide precipitates ranged from several to several dozen micrometres (Fig. 7). Additionally, the Cr_3C_2 phase, which constituted the cores of the larger Cr_3C_2 carbide particles, was visible on the cross sections of the melted coatings. These carbides were not completely transformed into Cr_7C_3 carbides. They were most visible in the zone

between the remelted and unmodified parts of the coating (Fig. 5f). Figure 7 shows the core of the original carbide particle, which has not undergone any transformation. The transformation of carbide occurred only in its external zone, where intense heating resulted in melting and diffusion of carbon into the matrix. Electron diffraction studies using TEM showed that, after laser remelting, Cr_7C_3 carbide was mainly formed during cooling, which indicates its easier crystallisation under these conditions compared to Cr_3C_2 carbide (Fig. 8). According to the C-Cr phase diagram, Cr_3C_2 carbide undergoes a peritectic transformation $\text{L} + \text{C} \leftrightarrow \text{Cr}_3\text{C}_2$ at a temperature of 1811 °C, while when cooling from the liquid phase to 1727 °C, a new Cr_7C_3 carbide phase can be formed (Ref 26). It should be emphasised that the processes occurring during laser remelting are not in equilibrium and do not always have to occur following the phase diagram. The grain-refined structure of the coating created in the laser melting process had a beneficial effect on its microhardness, showing an increase of approximately 20% compared to that before processing. Although Cr_7C_3 carbide has a lower hardness (18.3 GPa) than Cr_3C_2 (20.9 GPa) (Ref 27), the coating hardness increased significantly. This was influenced by the fine-grained structure of the coating after remelting and the microstructure consisting mainly of the Cr_7C_3 phase and the nickel–chromium matrix occurring in various forms, e.g. alternating lamellas of Cr_7C_3 carbides and the matrix, or the presence of carbides of various shapes in the matrix (Ref 28, 29). Moreover, the presence of the nanocrystalline structure of the coatings had a significant impact on improving their properties. Similar observations were reported by Roy et al. (Ref 30), Chong et al. (Ref 31) and Janka et al. (Ref 32), who showed a high density of fine and hard precipitates occurring in the nickel–chromium matrix, improving the properties of coatings. The higher hardness of the coatings corresponded to higher abrasion wear resistance and better tribological properties (less wear index) during the tests at 25 °C and 250 °C. Cold-sprayed (Cr_3C_2 -25(Ni20Cr))-5(Ni25C) coatings subjected to laser surface treatment showed approximately 30% lower weight loss (Fig. 10), compared to the as-sprayed ones. Wear index (W_v) determined during ball-on-disc tests have shown that laser-melted coatings are characterised by the lowest wear at 25 °C, regardless of the applied load (Fig. 11). During test, the Cr_3C_2 small particles detached from the coating material formed grooves, and therefore, at 25 °C, a wear index is higher for the as-sprayed deposit. Increasing the test temperature to 250 °C caused the metal matrix to be softer, and carbide particles ground against the wear path, creating larger grooves and furrows. Because the Cr_3C_2 carbides were more brittle than Cr_7C_3 and had greater ease of particles detaching, the wear of the cold-sprayed deposit was more intense. A temperature of 250 °C

is insufficient to form a tribofilm, which was responsible for a significant wear index reduction. During the ball-on-disc test at 500 °C, the actual temperature was significantly higher (even around 800 °C). This caused a greater amount of tribofilm to form, as a result, of the wear of the sample and the Si_3N_4 ball. The formed tribofilm acted as a lubricant, protecting the coating against wear, which was especially visible in the as-sprayed coatings, which revealed the lower wear index. The higher wear index of modified deposits was related to its appreciable softening. The more ductile modified coating with Cr_7C_3 carbides of different shapes resulted in faster abrasive wear at 500 °C compared to as-sprayed deposits containing Cr_3C_2 carbides. The improvement in tribological properties was influenced by both the grain refinement of the coating structure and the chromium oxide Cr_2O_3 layer formed on the surface, identified using TEM (Fig. 9). Chromium oxide layers reveal very good anti-abrasive properties, as shown by Mohammadtaheri et al. (Ref 33) in the case of magnetron sputtered coatings, and Dong et al. (Ref 33) in plasma-sprayed coatings. Particularly noteworthy is the fact that the laser-treated coatings were devoid of porosity (Fig. 5e), apart from a few holes occurring near their surface (Fig. 4(c), (a), and (d)). This distinguishes them from the group of coating materials obtained by other thermal spray methods (plasma or HVOF), where comparable mechanical properties were obtained (Ref 30, 31).

Conclusions

This work presents the characterisation of the laser-treated (Cr_3C_2 -25(Ni20Cr))-5(Ni25C) composite coatings cold-sprayed on the 1H18N9T steel substrate. The use of surface laser treatment enabled the development of new coating materials with increased properties in the near-surface zone of a certain thickness, below which the properties of cold-sprayed coatings were retained. The influence of a diode laser beam on the microstructure, surface topography and wear resistance of the deposits was analysed. The obtained results are shown below.

1. Cermet coatings were laser melted to a depth of 60%, without the presence of significant porosity.
2. The surface modification led to a phase composition change in the deposits, which, apart from $\text{Cr}_{0.25}\text{Ni}_{0.75}$ and Cr_3C_2 , revealed the presence of new phases, such as Cr_7C_3 carbide in their structure and an uneven thickness Cr_2O_3 oxide layer up to 200 nm on the surface.
3. The laser-treated coatings were characterised by the lowest wear index (W_v) at 25 °C and 30% lower mass loss during wear tests with loose abrasive and 20%

higher microhardness compared to the as-sprayed deposits.

4. The value of the friction coefficient was similar for all examined coatings and decreased with increasing temperature, except for the coating tested under a load of 15 N at 500 °C, regardless of the applied load.
5. The laser surface melting caused changes in the coating morphology and microstructure and significantly improved the mechanical and tribological properties of the cermet ($\text{Cr}_3\text{C}_2\text{-}25(\text{Ni}20\text{Cr})\text{-}5(\text{Ni}25\text{C})$).

Acknowledgment This work was supported by the National Science Centre, Poland (Project No 2017/25/B/ST8/02228).

Open Access This article is licensed under a Creative Commons Attribution 4.0 International License, which permits use, sharing, adaptation, distribution and reproduction in any medium or format, as long as you give appropriate credit to the original author(s) and the source, provide a link to the Creative Commons licence, and indicate if changes were made. The images or other third party material in this article are included in the article's Creative Commons licence, unless indicated otherwise in a credit line to the material. If material is not included in the article's Creative Commons licence and your intended use is not permitted by statutory regulation or exceeds the permitted use, you will need to obtain permission directly from the copyright holder. To view a copy of this licence, visit <http://creativecommons.org/licenses/by/4.0/>.

References

1. R. Fernandez and B. Jodoin, Effect of Particle Morphology on Cold Spray Deposition of Chromium Carbide-Nickel Chromium Cermet Powders, *J. Therm. Spray Technol.*, 2017, **26**, p 1356-1380.
2. A. Trelka, W. Żórawski, and A. Góral, Microstructure and Properties Modification of Cold Sprayed Coatings Using Different Grain Size of $\text{Cr}_3\text{C}_2\text{-}25(\text{Ni}20\text{Cr})$ Composite Powder, *Stroj Vestn-J Mech E*, 2020, **66**, p 494-504.
3. A. Góral, W. Żórawski, and M. Makrenek, The Effect of the Standoff Distance on the Microstructure and Mechanical Properties of Cold Sprayed $\text{Cr}_3\text{C}_2\text{-}25(\text{Ni}20\text{Cr})$ Coatings, *Surf. Coat. Technol.*, 2019, **361**, p 9-18.
4. D. Poirier, J.G. Legoux, and R. Lima, Engineering HVOF-Sprayed $\text{Cr}_3\text{C}_2\text{-NiCr}$ Coatings: the Effect of Particle Morphology and Spraying Parameters on the Microstructure, Properties and High Temperature Wear Performance, *J. Therm. Spray Technol.*, 2013, **22**(2-3), p 280-289.
5. S. Matthews, M. Hyland, and B. James, Long-Term Carbide Development in High-Velocity Oxygen Fuel/High-Velocity Air Fuel $\text{Cr}_3\text{C}_2\text{-NiCr}$ Coatings Heat Treated at 900 °C, *J. Therm. Spray Technol.*, 2004, **13**(4), p 526-536.
6. J.M. Guilemany, J.M. Miguel, S. Vizcaino, C. Lorenzana, J. Delgado and J. Sanchez, Role of Heat Treatments in the Improvement of the Sliding Wear Properties of $\text{Cr}_3\text{C}_2\text{-NiCr}$ Coatings, *Surf. Coat. Technol.*, 2002, **157**(2-3), p 207-213.
7. A. Trelka, W. Żórawski, Ł. Maj, P. Petrzak, D. Soboń, and A. Góral, The Effect of the Substrate on the Microstructure and Tribological Properties of Cold Sprayed ($\text{Cr}_3\text{C}_2\text{-}25(\text{Ni}20\text{Cr})\text{-}(\text{Ni-graphite})$) Cermet Coatings, *Materials*, 2022, **15**, p 994.
8. D.R. Eo, S.G. Chung, J. Yang, W.T. Cho, S.H. Park, and J.W. Cho, Surface Modification of High-Mn Steel via Laser-DED: Microstructural Characterization and Hot Crack Susceptibility of Clad Layer, *Mater. Des.*, 2022, **223**, 111188.
9. Y. Chen, F. Lu, K. Zhang, P. Nie, S.R. Hosseini, K. Feng, and Z. Li, Dendritic Microstructure and Hot Cracking of Laser Additive Manufactured Inconel 718 under Improved Base Cooling, *J. Alloys Compd.*, 2016, **15**(670), p 312-321.
10. L.H. Hu, J. Huang, Z.G. Li, and Y.X. Wu, Effects of Preheating Temperature on Cold Cracks, Microstructures and Properties of High Power Laser Hybrid Welded 10Ni3CrMoV Steel, *Mater. Des.*, 2011, **32**, p 1931-1939.
11. S. Zenitani, N. Hayakawa, J. Yamamoto, K. Hiraoka, Y. Morikage, T. Kubo, and K. Yasuda, Amano, Development of New Low Transformation Temperature Welding Consumable to Prevent Cold Cracking in High Strength Steel Welds, *Sci. Technol. Weld. Joi.*, 2007, **12**, p 516-522.
12. A. Góral, W. Żórawski, L. Lityńska-Dobrzyńska, M. Makrenek, M. Goły, A. Trelka, and M. Szezynger, Laser Modification of the Microstructure and Mechanical Properties of ($\text{Cr}_3\text{C}_2\text{-}25(\text{Ni}20\text{Cr})\text{-}5(\text{Ni}25\text{C})$) Cermet Coatings Containing a Solid Lubricant, *Surf. Coat. Technol.*, 2020, **405**, 126701.
13. P. Serra, J.M. Miguel, J.L. Morenza, and J.M. Guilemany, Structural Characterization of Laser-Treated $\text{Cr}_3\text{C}_2\text{-NiCr}$ Coatings, *J. Mater. Res.*, 2001, **16**, p 3416-3422.
14. J. Kusiński, S. Kaç, A. Kopia, A. Radziszewska, M. Rozmus-Górnikowska, B. Major, Ł. Major, J. Marczak, and A. Lisiecki, Laser Modification of the Materials Surface Layer—a Review Paper, *Bull. Pol. Acad. Sci. Tech.*, 2012, **60**(4), p 711-728.
15. M. Grimm, T. Lindner, and T. Lampke, Effects of Laser-Remelting on the Microstructure, Hardness and Oscillating Wear Resistance of Atmospheric Plasma Sprayed Alumina-Rich Coatings, *Coatings*, 2022, **12**, p 721.
16. J. Morimoto, Y. Sasaki, S. Fukuhara, N. Abe, and M. Tukamoto, Surface Modification of $\text{Cr}_3\text{C}_2\text{-NiCr}$ Cermet Coatings by Direct Diode Laser, *Vacuum*, 2006, **80**(11-12), p 1400-1405.
17. A. Gisario, M. Barletta, and F. Veniali, Laser Surface Modification (LSM) of Thermally-Sprayed Diamalloy 2002 Coating, *Opt. Laser Technol.*, 2012, **44**, p 1942-1958.
18. A. Trelka, A. Góral, W. Żórawski, T. Gancarz, and P. Petrzak, The Mechanical and Tribological Properties of Cold-Sprayed Cermet Coatings—Al Alloy Substrate Systems, *J. Therm. Spray Tech.*, 2023, **32**, p 1714-1727.
19. Geometrical Product Specifications (GPS)-Surface Texture: Areal-Part 2: Terms, Definitions and Surface Texture Parameters. ISO: Geneva, Switzerland, 2012, ISO 25178-2:2012
20. Metallic Materials—Vickers Hardness Test—Part 1: Test Method. International Organization for Standardization, Geneva, 2018, EN ISO 6507-1: 2018.
21. Fine Ceramics (Advanced Ceramics, Advanced Technical Ceramics) Determination of Friction and Wear Characteristics of Monolithic Ceramics by Ball-on-Disc Method, 2016, ISO 20808:2016(E).
22. S. Matthews, B. James, and M. Hyland, The Role of Microstructure in the Mechanism of High Velocity Erosion of $\text{Cr}_3\text{C}_2\text{-NiCr}$ Thermal Spray Coatings: Part 1—As-Sprayed Coatings, *Surf. Coat. Technol.*, 2009, **203**(8), p 1086-1093.
23. S. Matthews, B. James, and M. Hyland, Microhardness Variation in Relation to Carbide Development in Heat Treated $\text{Cr}_3\text{C}_2\text{-NiCr}$ Thermal Spray Coatings, *Acta Mater.*, 2003, **51**, p 4267-4277.
24. S. Matthews and L.M. Berger, Long-Term Compositional/Microstructural Development of $\text{Cr}_3\text{C}_2\text{-NiCr}$ Coatings at 500 °C, 700 °C and 900 °C, *Int. J. Refract. Hard. Met.*, 2016, **59**, p 1-18.
25. J. He and E.J. Lavernia, Precipitation Phenomenon in Nanostructured $\text{Cr}_3\text{C}_2\text{-NiCr}$ Coatings, *Mater. Sci. Eng. A*, 2001, **301**, p 69-79.

26. M. Venkatraman and J.P. Neumann, The C-Cr (Carbon-Chromium) System, *Bull. Alloy Phase Diagr.*, 1990, **11**(2), p 152-159.
27. Y. Li, Y. Gao, B. Xiao, T. Min, Y. Yang, S. Ma, and D. Yi, The Electronic, Mechanical Properties and Theoretical Hardness of Chromium Carbides by First-Principles Calculations, *J. Alloys Compd.*, 2011, **509**(17), p 5242-5249.
28. T. Tomita, Y. Takatani, K. Tani, and Y. Harada, Mechanisms of High Hardness in Cr₃C₂-NiCr Cermet Coatings Formed by Vacuum Plasma Spraying, *Therm. Spray.*, 2001, **28**, p 699-704.
29. W. Mayr, W. Lengauer, P. Etmayer, D. Rafaja, J. Bauer, and M. Bohn, Phase Equilibria and Multiphase Reaction Diffusion in the Cr-C and Cr-N Systems, *J. Phase Equilib.*, 1999, **20**(1), p 35-44.
30. M. Roy, A. Pauschitz, J. Bernardi, T. Koch, and F. Franek, Microstructure and Mechanical Properties of HVOF Sprayed Nanocrystalline Cr₃C₂-25(Ni20Cr) Coating, *J. Therm. Spray Tech.*, 2006, **15**, p 272-381.
31. K. Chong, Y. Zou, D. Wu, Y. Tang, and Y. Zhang, Pulsed Laser Remelting Supersonic Plasma Sprayed Cr₃C₂-NiCr Coatings for Regulating Microstructure, Hardness and Corrosion Properties, *Surf. Coat. Technol.*, 2021, **418**, 127258.
32. L. Janka, J. Norpoth, R. Trache, S. Thiele, and L.-M. Berger, HVOF- and HVAF-Sprayed Cr₃C₂-NiCr Coatings Deposited from Feedstock Powders of Spherical Morphology: Microstructure Formation and High-Stress Abrasive Wear Resistance up to 800 °C, *J. Therm. Spray Tech.*, 2017, **26**, p 1720-1731.
33. M. Mohammadtaheri, Q. Yang, Y. Li, and J. Corona-Gomez, The Effect of Deposition Parameters on the Structure and Mechanical Properties of Chromium Oxide Coatings Deposited by Reactive Magnetron Sputtering, *Coatings*, 2018, **8**, p 111.
34. S. Dong, S. Song, B. Hanasz, H. Liao, and C. Coddet, Improvement in the Microstructure and Property of Plasma Sprayed Metallic, Alloy and Ceramic Coatings by Pre-/During-Treatment of Dry-Ice Blasting, *Surf. Coat. Technol.*, 2013, **220**, p 199-203.

Publisher's Note Springer Nature remains neutral with regard to jurisdictional claims in published maps and institutional affiliations.